

# The Detection of a Cooling Flow Elliptical Galaxy from O VI Emission

Joel N. Bregman, Eric D. Miller, and Jimmy A. Irwin  
*Dept. of Astronomy, University of Michigan, Ann Arbor, MI 48109-1090*

## ABSTRACT

Cooling flow models for the hot gas in elliptical galaxies predict that gas is cooling at a rate of  $\sim 1 M_{\odot} \text{ yr}^{-1}$ , yet there is little evidence for this phenomenon beyond the X-ray waveband. If hot gas is cooling, it will pass through the  $3 \times 10^5 \text{ K}$  regime and radiate in the O VI  $\lambda\lambda 1032, 1038$  ultraviolet lines, which can be detected with the *Far Ultraviolet Spectroscopic Explorer (FUSE)* and here we report on *FUSE* observations of the X-ray bright early-type galaxies NGC 1404 and NGC 4636. In NGC 1404, the O VI doublet is not detected, implying a cooling rate  $< 0.3 M_{\odot} \text{ yr}^{-1}$ , which is below the predicted values from the cooling flow model of  $0.4\text{--}0.9 M_{\odot} \text{ yr}^{-1}$ . In NGC 4636, both O VI lines are clearly detected, indicating a cooling rate of  $0.43 \pm 0.06 M_{\odot} \text{ yr}^{-1}$ , which falls within the range of values from the cooling flow prediction,  $0.36\text{--}2.3 M_{\odot} \text{ yr}^{-1}$  and is closest to the model where the production of the cooled gas is distributed through the galaxy. The emission line widths,  $44 \pm 15 \text{ km s}^{-1}$ , are close to the Doppler broadening value ( $30 \text{ km s}^{-1}$ ), indicating that the flow is quiescent rather than turbulent, and that the flow velocity is  $< 30 \text{ km s}^{-1}$ .

*Subject headings:* galaxies: individual (NGC 1404, NGC 4636) — galaxies: ISM

## 1. Introduction

In the standard model for cooling flow ellipticals, the gas shed by stars during normal stellar evolution becomes thermalized, colliding with ejecta from other stars and with the ISM. This process heats the gas to  $10^{6.5}\text{--}10^7 \text{ K}$ , and if there were no additional heating or cooling, the gas would be bound to the galaxy and have the same spatial distribution as the stars. However, radiative cooling drains energy from the gas most rapidly at small radii, causing a loss of buoyancy and a subsequent inflow of gas. The rate at which gas cools and flows inward ( $\dot{M}$ ) is proportional to two observed quantities, the energy loss rate ( $L_X$ ) divided by the thermal energy per gram ( $3kT_X/\mu m_p$ ), or  $\dot{M} \propto L_X/T_X$ , typically  $0.03\text{--}3 M_{\odot} \text{ yr}^{-1}$  for ellipticals.

Although cooling flow models do an adequate job in explaining the X-ray data, there is little confirmation for the consequences of the models. In particular, the cooling flow will produce cooled

gas, yet gas at  $\lesssim 10^4 \text{ K}$  is not seen in abundance in these systems (Roberts et al. 1991), suggesting that the gas is turned into stars. However, if stars are produced with a normal initial mass function, young blue stars would have been detected if the rate was above  $0.01 M_{\odot} \text{ yr}^{-1}$  (O’Connell 1999). Therefore, either star formation in these systems does not produce many stars above  $1 M_{\odot}$ , or the basic model is wrong. Most of the modifications to the basic model involve some sort of heating mechanism to balance the radiative cooling and prevent cool gas from being produced. The critical issue is whether the gas is losing its thermal energy and a simple test is to search for the emission lines that are produced as gas cools through intermediate temperatures.

The most powerful diagnostic line for such a test is the O VI doublet, which is produced as the gas passes through the  $3 \times 10^5 \text{ K}$  range, at which point the gas has lost 90–95% of its original thermal energy, so it has effectively cooled. As gas cools through the  $2\text{--}4 \times 10^5 \text{ K}$  range, the

cooling is carried by a single ionization state of a single element, O VI, and its doublet lies at  $\lambda\lambda 1032, 1038$ , now accessible with the *Far Ultraviolet Spectroscopic Explorer (FUSE)*. The relationship between line luminosity and cooling rate ( $\dot{M}$ ) is insensitive to the metallicity of the gas or to whether the gas is out of equilibrium (Edgar and Chevalier 1986). Consequently, the luminosity of the  $\lambda\lambda 1032, 1038$  lines is a direct measure of  $\dot{M}$ . We have a program using *FUSE* (Moos et al. 2000) to observe cooling flow ellipticals and here we report on the first two observations, which are of the classic cooling flow galaxies NGC 4636 and NGC 1404.

## 2. Observations

Out of a more extensive program, NGC 1404 and NGC 4636 are the first two galaxies to be observed, and they are X-ray bright, so their emission is dominated by hot gas (e.g., Canizares, Fabiano, and Trinchieri 1987). Furthermore, the cooling time of the X-ray emitting gas is far less than a Hubble time, making these classic cooling flow galaxies. There are important differences between these two galaxies in their optical luminosity as well as their X-ray to optical luminosity ratio, leading to different values for the mass cooling rate  $\dot{M}$ . The galaxy NGC 1404 is in the Fornax cluster and for a distance of 28.4 Mpc ( $H_o = 50 \text{ km s}^{-1} \text{ Mpc}^{-1}$ ; the conclusions are distant independent),  $\log L_B = 10.74$ ,  $\log L_X = 41.27$  and  $T_X = 0.56 \text{ keV}$  (Faber et al. 1989; Brown and Bregman 2000), while NGC 4636 is in the outskirts of the Virgo cluster with a distance of 26.7 Mpc and with properties  $\log L_B = 10.96$ ,  $\log L_X = 41.81$  and  $T_X = 0.72 \text{ keV}$ .

The observations for NGC 1404 were obtained in 10 December 1999, with an exposure time of 7.49 ksec, while the data for NGC 4636 were obtained in 23 May 2000 with an exposure time of 6.46 ksec. In both cases, the large aperture was used, which is  $30''$  square, leading to a velocity resolution of  $100 \text{ km s}^{-1}$ ; there is no effective spatial information perpendicular to the dispersion axis. The data streams did not contain periods of bursts or other detrimental events, so editing of the event file was not necessary. The data were processed with the pipeline program during January 2001, including an optimal extraction algo-

rithm, which uses a local background and employs information about the shape of the spectrum perpendicular to direction of the spectrum. Four different detector segments cover the spectral region of interest, two LiF segments and two SiC segments, but the LiF1a channel had the highest  $S/N$  and was used in most of the analysis. Addition of the other channels generally reduced the  $S/N$  and led to spurious features in the spectrum. The  $30''$  aperture was centered on the optical centers of the galaxies and the resulting spectra around the regions of the O VI emission in NGC 4636 and NGC 1404 are shown in Figures 1 and 2.

These spectra have features not associated with the elliptical galaxies, such as airglow lines and Galactic absorption lines. These lines of sight are out of the plane of the Milky Way, where the H I columns are  $1.36 \times 10^{20} \text{ cm}^{-2}$  (NGC 1404) and  $1.63 \times 10^{20} \text{ cm}^{-2}$  (NGC 4636), and at these low values, the H<sub>2</sub> absorption lines are not expected to be large. The strongest Galactic atomic line in the region is that of C II at  $1036.34 \text{ \AA}$ , followed by O I lines at  $1026.47 \text{ \AA}$  and  $1039.23 \text{ \AA}$ . A few other lines fall in this window, the ground-state doublet of O VI  $\lambda\lambda 1031.95, 1037.63$  and the excited metastable line C II\*  $\lambda 1037.02$ , and although Galactic absorption by these lines is seen in a number of other sightlines through the galaxy (e.g., Sembach et al. 2000), they are weaker. These two O VI lines are the ones predicted to be present in cooling flows in emission, and for optically thin conditions, the O VI  $\lambda 1032$  line will be twice as strong as the O VI  $\lambda 1038$  line.

### 2.1. NGC 1404

Of the four segments, only the LiF1a had a count rate above the background rate and it produces the highest  $S/N$  spectrum in the  $1025\text{--}1050 \text{ \AA}$  range (Fig. 2). The spectrum in the range  $1025\text{--}1050 \text{ \AA}$  range shows a stellar continuum upon which terrestrial airglow lines plus a few Galactic absorption features are present (Fig. 2): the strong line of C II  $\lambda 1036.34$  at zero velocity; an O I  $\lambda 1026.47$  line adjacent to the Ly $\beta$  airglow feature; and Ly $\beta$  absorption, although it is filled in by the Ly $\beta$  airglow line plus two other airglow lines at  $1027\text{--}1028 \text{ \AA}$ . Given the modest intensity of the airglow line at  $1025.5 \text{ \AA}$ , the other airglow lines in this spectral region should be unimportant, and they are generally not visible (e.g., the O I  $\lambda 1039.2$

line is absent). The strongest  $H_2$  lines in this and other spectral regions are not visible, so the Galactic  $N(H_2) < 10^{18} \text{ cm}^{-2}$ . There are no interstellar atomic or molecular absorption lines at the redshift of NGC 1404.

The stellar continuum has one dominant feature in Figure 2,  $Ly\beta$  absorption, plus a number of minor absorption lines. In an effort to understand which features are stellar and which might be interstellar, we can compare it to an appropriate stellar model. As discussed by O’Connell (1999), the continuum in this region is produced by low mass stars that either populate the extreme horizontal branch or have evolved away from it. Models that include these various stellar contributions were calculated by Brown et al. (1997) for comparison with HUT data, with atmospheric metallicities of  $0.1Z_\odot$  leading to the best fits. These low atmospheric abundances probably reflect diffusion processes since the mean metallicities of the stars in these systems are near-solar. The model of Brown et al. (1997) is at  $3 \text{ \AA}$  resolution, which is too low for comparison with our data, so instead we use the average of two stars of different gravity ( $g = 4, 5.5$ ), as these are representative of the range of gravities for the stars that contribute to the flux in this wavelength region (Dorman, Rood, and O’Connell 1993); we used a surface metallicity of  $0.1Z_\odot$  and  $T = 26,000 \text{ K}$ . Also, this model was convolved with the velocity dispersion of the galaxy (Fig. 2).

The expected O VI emission lines from NGC 1404 would be shifted to  $\lambda\lambda 1038.6, 1044.3 \text{ \AA}$  ( $1947 \text{ km s}^{-1}$ ), and relative to the continuum, there is no evidence of emission from either line. To estimate the upper limit to the line strength, we assume that the line width is characteristic of the velocity dispersion of the system,  $\Delta\lambda = 1.0 \text{ \AA}$  ( $300 \text{ km s}^{-1}$ ). Conservative  $3\sigma$  upper limits for the lines are  $F(\lambda 1032) < 3 \times 10^{-15} \text{ erg cm}^{-2} \text{ s}^{-1}$ , and  $F(\lambda 1038) < 1.4 \times 10^{-15} \text{ erg cm}^{-2} \text{ s}^{-1}$ . The extinction in this region is very low, estimated to be  $A_V = 0.00-0.05$ , so the average would lead to a extinction correction of a factor of 1.08 at  $1035 \text{ \AA}$ .

## 2.2. NGC 4636

The spectrum of NGC 4636 contains two Galactic features seen in the spectrum of NGC 1404, the C II  $\lambda 1036.34$  and the O I  $\lambda 1039.23$  feature (Fig. 1), although they are shifted by  $0.24 \text{ \AA}$  and  $0.30$

$\text{\AA}$  respectively from their rest wavelengths (about  $+70 \text{ km s}^{-1}$ ). These Galactic absorption lines are expected to occur near  $0 \text{ km s}^{-1}$ , yet there is no line at this location with the instrumental width. Also there is no known Galactic H I feature of any importance at  $+70 \text{ km s}^{-1}$ , which would need to dominate the neutral column in this direction to cause the observed results. Instead, it appears that there is a spectral shift of about  $0.3 \text{ \AA}$ , and a similar shift is seen in the  $Ly\beta$  airglow line, which is redshifted by  $0.40 \text{ \AA}$ . Consequently, in our analysis, we apply a shift to the data of  $-0.3 \text{ \AA}$  ( $-87 \text{ km s}^{-1}$ ). In addition to the atomic lines, there is modest absorption by  $H_2$ , although only the strongest lines are detected, such as the  $1049.7 \text{ \AA}$  line. Based on the strength of this and other Galactic  $H_2$  (e.g., in the  $1062.5-1064 \text{ \AA}$  region), we estimate that  $N(H_2) \approx 10^{18.5} \text{ cm}^{-2}$ , typical of lines of sight with this  $N(\text{H I})$  value.

Aside from the absorption lines and airglow lines, the two strongest features are emission lines that correspond to the wavelengths at which the O VI doublet would occur near the redshift of NGC 4636; the line centers are  $1018 \pm 20 \text{ km s}^{-1}$  ( $\lambda 1032$  line) and  $1061 \pm 20 \text{ km s}^{-1}$  ( $\lambda 1038$  line) compared to the galaxy redshift of  $938 \pm 4 \text{ km s}^{-1}$  (from NED). The separation of the line peaks is, to within the errors, consistent with the separation of the two lines in the O VI, but the mean velocity of the lines is  $100 \text{ km s}^{-1}$  greater than that expected. This difference may result from wavelength calibration errors since in a previous version of the pipeline processing, the wavelength of the O VI was consistent with optical redshift for NGC 4636.

The two lines are single-peaked and fairly narrow. The FWHM of the lines are about  $0.15 \pm 0.05 \text{ \AA}$  ( $44 \text{ km s}^{-1}$ ), with the error depending upon where one defines the continuum. The instrumental resolution depends upon the degree to which the aperture is illuminated. The airglow lines, which fill the aperture uniformly, have a FWHM of  $0.34 \text{ \AA}$  ( $100 \text{ km s}^{-1}$ ), while a point source would have a FWHM of about  $0.05 \text{ \AA}$  ( $15 \text{ km s}^{-1}$ ). Therefore, the emission lines from NGC 4636 must not fill the aperture uniformly, although we cannot determine whether the line width is due to an instrumental limitation or to Doppler broadening. The line fluxes are  $F(\lambda 1032) = 3.0 \pm 0.6 \times 10^{-15} \text{ erg cm}^{-2} \text{ s}^{-1}$ , and  $F(\lambda 1038) = 2.4 \pm 0.6 \times 10^{-15}$

erg cm<sup>-2</sup> s<sup>-1</sup>, with the primary error in the line fluxes resulting from the uncertain placement of the continuum. The line ratio,  $1.25 \pm 0.32$ , is  $2.3\sigma$  from the optically thin value of 2.0, but given the uncertainty in the model stellar continuum, we do not consider this difference particularly significant. The extinction along this sight-line is  $A_V = 0.04\text{--}0.09$ , depending upon the reddening model used (Burstein and Heiles 1982, or Schlegel, Finkbeiner, and Davis 1998), so we use the average of the two values, along with a value of  $A(1035 \text{ \AA})/A_V = 4.0$  (Cardelli et al. 1989), which leads to an extinction-corrected value of  $F(\lambda 1032 + \lambda 1038) = 6.8 \pm 0.9 \times 10^{-15}$  erg cm<sup>-2</sup> s<sup>-1</sup>.

### 3. Interpretation and Discussion

The conversion between the O VI line luminosity and cooling rate depends only weakly on the details of the physical situation, provided that the initial temperature is significantly higher than the temperature at which the ion is most abundant. This situation occurs in these galaxies, where the ambient temperature of the hot X-ray emitting gas is  $6\text{--}9 \times 10^6$  K and the ionization fraction in O VI is negligible. The cooling of the gas will proceed isobarically if the cooling time is long compared to the sound-crossing time of the region, eventually becoming isochoric as the gas cools and the relative size of the timescales is reversed. If gaseous cooling occurs in regions smaller than 1 kpc, the transition from the isobaric to isochoric case occurs at  $T \lesssim 4 \times 10^5$  K (Edgar and Chevalier 1986), and the cooling may be entirely isobaric as it applies to O VI. Unfortunately, we do not at this time have a good constraint on the size of the cooling region. For the pure isobaric case, Edgar and Chevalier (1986) show that  $L(\lambda 1032) = 1.1 \times 10^{39} \dot{M}$  erg s<sup>-1</sup> ( $\dot{M}$  is in  $M_\odot$  yr<sup>-1</sup>) and for the pure isochoric case,  $L(\lambda 1032) = 0.7 \times 10^{39} \dot{M}$  erg s<sup>-1</sup> (the  $\lambda 1038$  line is half of the strength of the  $\lambda 1032$  line). In this paper, we will use a conversion that is halfway between the isochoric and isobaric cases,  $L(\lambda 1032) = 0.9 \times 10^{39} \dot{M}$  erg s<sup>-1</sup>, which introduces only a 20% uncertainty in the model; the resulting values of  $\dot{M}$  are given in Table 1.

The critical test is to compare these values of  $\dot{M}$  with those derived from X-ray measurements. The cooling rate  $\dot{M}$  is the rate at which the thermal en-

ergy of the system is being drained away by radiative losses, so it is the ratio of the net cooling rate divided by the specific thermal energy content, or  $\dot{M} = L_{net}/E$ , where the specific thermal energy is  $E = 3kT/\mu m_p$ ,  $\mu$  is the mean molecular weight for the hot gas ( $\mu = 0.63$ ) and  $m_p$  is the usual proton mass. The net energy loss rate  $L_{net}$  equals the radiative loss rate (the bolometric X-ray luminosity) minus heating sources such as supernovae or gravitational compression as the gas falls inward. The amount of gravitational compressional heating depends upon whether the gas cools close to where it entered the flow or whether it flows into the central region ( $r \lesssim r_{core}$ ) before losing most of its thermal energy. The gas will become cool only in the central region unless thermal instabilities can grow throughout the flow, but the best calculations on this matter indicate that most linear perturbations will not grow rapidly enough to be effective (Balbus 1988). However, models without distributed mass drop-out lead to an X-ray surface brightness profile that is too sharply peaked in the center, inconsistent with observations. Consequently, most models include mass drop-out as a function of radius and the usual formulation is that the rate of mass drop-out is inversely proportional to the cooling time, or  $\dot{\rho} = q\rho/t_c$ , where  $t_c$  is the isobaric cooling time (Sarazin and Ashe 1989).

Without mass drop-out,  $q = 0$ , and a moderately efficient rate of drop-out would be given by  $q = 1$ , so we consider both cases. We use the model from Sarazin and Ashe (1989), where  $L_B = 1 \times 10^{11} L_\odot$ , and expressing  $L_X$  in units of  $10^{41}$  erg s<sup>-1</sup> and  $T_X$  in keV, we obtain  $\dot{M} = 0.26 L_X T_X^{-1} M_\odot$  yr<sup>-1</sup> for  $q = 0$ , and  $\dot{M} = 0.40 L_X T_X^{-1} M_\odot$  yr<sup>-1</sup> for  $q = 1$  (this is for the absorption-corrected X-ray luminosity in the 0.5–2.0 keV band). In the  $q = 1$  case, the mass drop-out occurs throughout the galaxy and since our 30'' square aperture does not encompass the entire galaxy, we must determine  $\dot{M}$  within the aperture. For our two galaxies, the square aperture encloses the emission from the galaxy within about 2.2 kpc (NGC 4636) and 2.4 kpc (NGC 1404) from the center, and in the  $q = 1$  model, this would enclose about half of the total  $\dot{M}$ . After applying this factor to the  $q = 1$  case, the resulting  $\dot{M}$  is similar to the  $q = 0$  case, with  $\dot{M} = 0.20 L_X T_X^{-1} M_\odot$  yr<sup>-1</sup>. We use the values of  $L_X$  and  $T_X$  given in Brown and Bregman (2000) for these galaxies to calculate values of  $\dot{M}$  for the

$q = 0$  case and for the  $q = 1$  case for the cooling only within the aperture (denoted  $\dot{M}_0$ ,  $\dot{M}_1$  and given in Table 1).

An alternative method of determining the expected value of  $\dot{M}$  is to use the X-ray observations directly by noting that  $\dot{\rho} = q\rho/t_c \propto \rho^2/\Lambda(T_X)$ , but since the cooling function  $\Lambda(T_X)$  changes far less than  $\rho$  in these galaxies, a good approximation is  $\dot{\rho} \propto \rho^2$ , and the amount of cooling gas in the aperture is the product of the line integral of  $\dot{\rho}$  through the galaxy, or  $\dot{M} \propto A \int \rho^2 dl$ , where  $A$  is the area of the aperture. The quantity  $\int \rho^2 dl$  is the emission measure, to which the X-ray surface brightness is proportional, so the fractional amount of  $\dot{M}$  within the aperture is just  $\dot{M}_A/\dot{M}_{Tot} = L_{X,A}/L_{X,Tot}$ . We have calculated the quantity  $L_{X,A}/L_{X,Tot}$  directly from the ROSAT PSPC data for these systems (using the backgrounds discussed by Brown and Bregman 2000) and obtain the fractional cooling within the *FUSE* aperture to be 0.083 (NGC 4636) and 0.25 (NGC 1404). This leads to values of  $\dot{M}$  within the apertures of  $0.36 M_\odot \text{ yr}^{-1}$  (NGC 4636) and  $0.40 M_\odot \text{ yr}^{-1}$  (NGC 1404), which is the product of  $L_{X,A}/L_{X,Tot}$  and the value of  $\dot{M}$  given above for the  $q = 1$  case (given as  $\dot{M}_2$  in Table 1). For NGC 1404, this value of the cooling rate in the aperture is within a factor of two of that derived entirely from the Sarazin and Ashe model. However, in the case of NGC 4636, the two values differ by up to a factor of six. Probably, this difference arises because NGC 4636 is more extended than the average galaxy of similar optical luminosity. Whereas NGC 4636 and NGC 1404 are similar in both optical luminosity and distance, NGC 4636 has a value for the half-light radius,  $r_e$ , that is nearly four times greater than for NGC 1404 (101'' compared to 27''). Consequently, the core radius used in the model by Sarazin and Ashe (1989) may be too small in the case of NGC 4636 and this would lead to an over-estimation of the fractional amount of  $\dot{M}$  within the aperture for the  $q = 1$  case; the values of  $\dot{M}$  are not affected for the  $q = 0$  case. The different values for  $\dot{M}$  from the X-ray data may be regarded as the expected range in the prediction, given the uncertainties in the models.

#### 4. Conclusions

For NGC 4636, the value of  $\dot{M}$  from the O VI measurement lies within the predicted range of  $\dot{M}$  from the X-ray data, lending strong support to the cooling flow model. Furthermore, the O VI result indicates a cooling rate significantly below that predicted from the  $q = 0$  model, a discrepancy that is removed if we assume that the cooling is distributed throughout the galaxy, which also was predicted from the application of the cooling flow models to the X-ray surface brightness distribution. Since  $\dot{M}(\text{O VI}) \approx \dot{M}_2$ , the mass dropout is consistent with that obtained by assuming that  $\dot{M}(< r) \propto L_X(< r)$ , although more detailed models providing determinations of  $\dot{M}$  should be calculated for NGC 4636, such as along the lines of Bringenti and Mathews (1996, 1999), who include a more accurate galaxy model plus important effects of accretion within the galaxy group.

In NGC 4636, the O VI line width of  $44 \pm 15 \text{ km s}^{-1}$  is similar to the thermal Doppler width of  $29 \text{ km s}^{-1}$  and is less than either the sound speed in the gas,  $77 \text{ km s}^{-1}$ , or the velocities of the  $10^4 \text{ K}$  optical emission line gas of  $200 \text{ km s}^{-1}$  (Caon et al. 2000). The narrow line width has several implications, the first being that the radial velocities within the cooling flow are less than  $30 \text{ km s}^{-1}$  ( $3 \sigma$  upper limit). This is consistent with the cooling flow calculations, which predict typical flow velocities of  $\sim 10 \text{ km s}^{-1}$  (e.g., Sarazin and Ashe 1989). Furthermore, the environment of the O VI gas must be quiescent, also consistent with models.

In contrast to NGC 4636, for NGC 1404 the predictions of the cooling flow model are not confirmed in the O VI data, where our upper limit is below the lowest X-ray prediction for  $\dot{M}$ . The most likely resolution of this discrepancy is that the net radiative loss rate is not given by the X-ray luminosity, which will occur if there is an additional source of heating, such as from supernovae or a central AGN. There is no evidence for a central radio source, as there is only an upper limit to the radio continuum emission of  $0.7 \text{ mJy}$  (6 cm; Sadler, Jenkins, and Kotanyi 1989).

In the future, we will observe additional galaxies to determine whether the cooling flow model is generally applicable. Also, we will obtain additional observations of NGC 4636 in off-central

locations, in order to determine the radial distribution of the cooling material, which is vital to modelers and to the determination of the location of the deposition of cooled gas that may produce new stars.

We would like to thank the considerable efforts of the *FUSE* staff in carrying out the observations and assisting us with the data processing; we received invaluable assistance from B-G Anderson, G. Sonneborne, W. Oegerle, J. Kruk, K. Sembach, and W. Blair. Also, we wish to acknowledge the insights and advice provided by W.G. Mathews, R. Edgar, R. O'Connell, T. Brown, and B. McNamara. Support for this program was provided by NASA through grant NAG5-9021.

## REFERENCES

- Balbus, S.A. 1988, *ApJ*, 328, 395
- Brighenti, F., and Mathews, W.G. 1996, *ApJ*, 470, 747
- Brighenti, F., and Mathews, W.G. 1999, *ApJ*, 512, 65
- Brown, B.A., and Bregman, J.N. 2000, *ApJ*, 539, 292
- Brown, T.M., Ferguson, H.C., Davidsen, A.F., and Dorman, B. 1997, *ApJ*, 482, 685
- Burstein, D., and Heiles, C. 1982, *AJ*, 87, 1165.
- Caon, N., Macchetto, D., and Pastoriza, M. 2000, *ApJS*, 127, 39
- Canizares, C.R., Fabbiano, G., and Trinchieri, G. 1987, *ApJ*, 312, 503
- Cardelli, J.A., Clayton, G.C., and Mathis, J.S. 1989, *ApJ*, 345, 245
- Dorman, B., Rood, R.T., and O'Connell, R.W. 1993, *ApJ*, 419, 596
- Edgar, R.J., and Chevalier, R.A. 1986, 310, L27
- Faber, S.M. et al. 1989, *ApJS*, 69, 763
- Moos, H.W., et al. 2000, *ApJL*, 538, L1
- O'Connell, R.W. 1999, *ARAA*, 37, 603
- Roberts, M.S., Hogg, D.E., Bregman, J.N., Forman, W.R., and Jones, C. 1991, *ApJS*, 75, 751
- Sadler, E.M., Jenkins, C.R., and Kotanyi, C.G. 1989, *MNRAS*, 240, 591
- Sarazin, C.L. and Ashe, G.A. 1989, *ApJ*, 345, 22
- Schlegel, D.J., Finkbeiner, D.P., and Davis, M. 1998, *ApJ*, 500, 525.
- Sembach, K.R., et al. 2000, *ApJL*, 538, L31

TABLE 1  
COOLING RATES FROM X-RAY AND O VI OBSERVATIONS.<sup>a</sup>

Galaxy Name	$\dot{M}(\text{O VI})$	$\dot{M}_0$	$\dot{M}_1$	$\dot{M}_2$
NGC 1404	$< 0.3$	0.86	0.66	0.40
NGC 4636	$0.43 \pm 0.06$	2.3	1.8	0.36

<sup>a</sup>Units of  $\dot{M}$  are  $M_{\odot} \text{ yr}^{-1}$ .

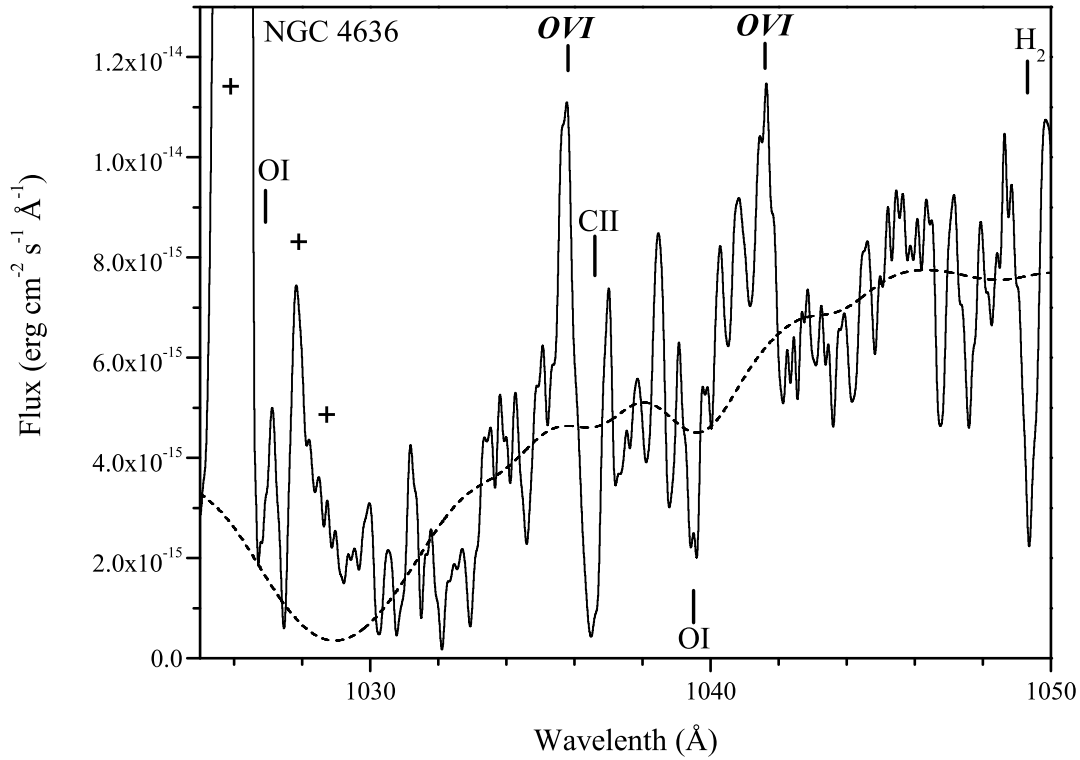


Fig. 1.— The FUSE spectrum of NGC 4636 in the 1020–1050 Å region shows airglow lines (notably  $\text{Ly}\beta$ ; denoted by +), several Galactic absorption lines, the strongest being C II (1036.34 Å) and O I (1026.47 Å, 1039.23 Å), and possibly O VI (1032 Å), as well as the redshifted O VI emission lines of from NGC 4636 (in italics). The dashed line is the expected stellar continuum from NGC 4636. The spectrum has been smoothed to a velocity resolution of  $100 \text{ km s}^{-1}$  for display purposes, although from the full resolution data, the O VI emission lines have a FWHM of  $44 \text{ km s}^{-1}$ , close to the thermal width of  $30 \text{ km s}^{-1}$ .

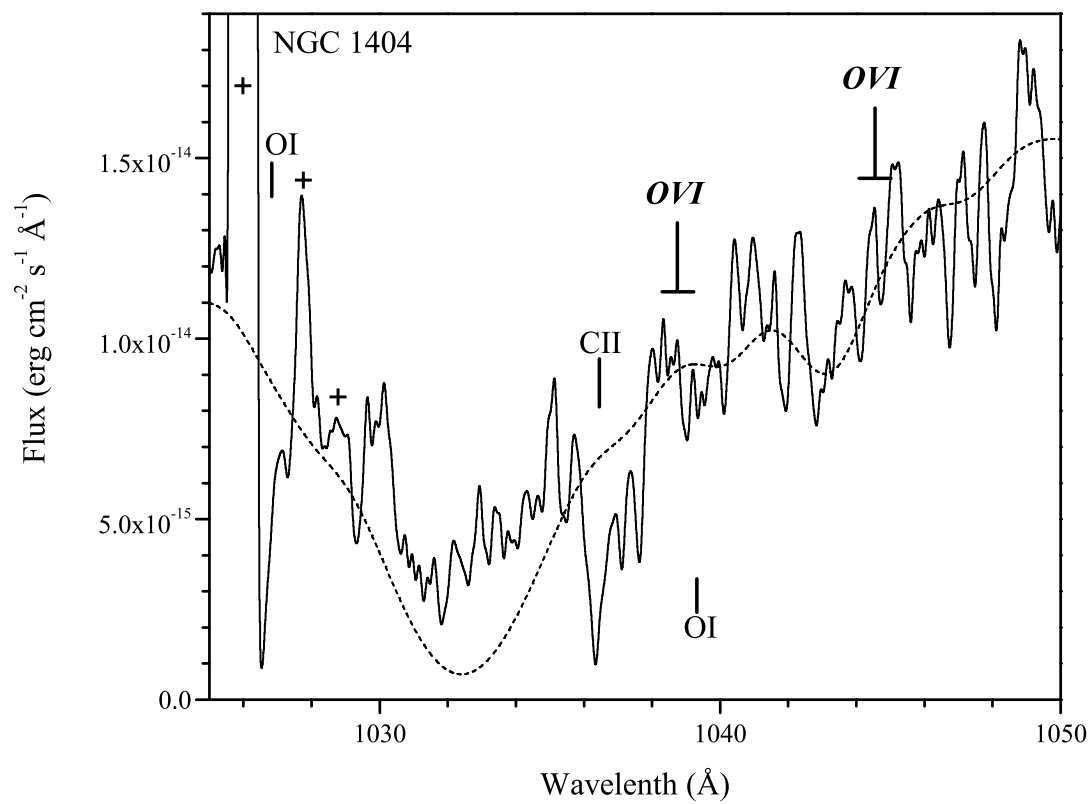


Fig. 2.— The FUSE spectrum of NGC 1404, similar to that in Figure 1, except there is no apparent detection of the redshifted O VI emission lines from NGC 1404.